Anisotropy of structural models for amorphous materials*

R. Alben and G. S. Cargill, III[†]

Department of Engineering and Applied Science, Yale University, New Haven, Connecticut 06520

J. Wenzel[‡]

Physics Department, University of Kent, Canterbury, England

(Received 6 August 1975)

Correlations responsible for anisotropic-scattering properties of close-packed and tetrahedrally coordinated amorphous-model structures are discussed. It is shown that although there are regular planes of high density associated with the strong-scattering directions, the scattering anisotropy is not very different from that which occurs for random scattering.

I. INTRODUCTION

The first insights into microscopic order in amorphous materials were obtained nearly fifty years ago from analysis of x-ray scattering measurements.[1] Such x-ray measurements, as well as similar measurements with electrons and neutrons, give a Fourier transform of correlations among atomic positions. For most amorphous materials, the scattering from a macroscopic volume is isotropic, i.e., independent of the orientation of the sample with respect to the scattering vector. Such scattering measurements can be inverted to obtain the radical distribution function[2] (RDF), which is presently the only direct measure of spatial correlations among atoms in amorphous materials. However, the RDF does not contain enough information to completely characterize the atomic scale structure; information about the directional properties of local correlations has been lost. Recently it has become possible to observe anisotropy in electron scattering from small areas of amorphous films,[3] and to obtain images which report the difference in scattering from different microscopic regions.[4-6] Although there is clearly added information in these results, there is as yet no systematic procedure to extract it.[7-9]

In this paper we discuss the anisotropy of scattering for several model structures for amorphous materials. The models have been constructed either manually or by computer and contain between 500 and 8000 atomic units.[10-15] Since we know the positions of all the atoms of these models, we may investigate in detail the spatial correlations which are associated with strong and with weak scattering directions. Previous studies of anisotropy in models for atomic arrangements in amorphous solids have been reported by Shevchik,[16] Chaudhari *et al*,[17,18] and Graczyk and Chaudhari.[19-22] The present report extends this previous work by examining more quantitatively the strength of anisotropies in many different models, by calling attention to the multiaxial nature of anisotropies in these models, and by demonstrating that anisotropies found in these models can be related to the anisotropies expected from randomly occurring reinforcement and interference in models consisting of random arrays of points.

We find, as might be expected, that there are regular density oscillations perpendicular to strong-scattering directions. However, these are not describable as local regions where atoms are stacked in a unique set of planes. Rather there are several families of planes going through a given model. The planes do not seem to terminate at well-defined boundaries, but rather in some cases correlations can be seen across the largest models studied. We interpret these results by comparing them with expectations for two extreme cases: (i) randomly occurring interference and reinforcement, and (ii) well-defined crystalline periodicities. For the models studied we find that the scattering anisotropy is within 40% of that expected for random interference and reinforcement.

We do not present here a definitive procedure for interpreting electron micrographs relating to scattering anisotropy. As Cochran and others have shown,[6,7,9] this would require careful considerations of instrumental factors as well as of atomic correlations. However, we believe that considerations of statistical variations of correlations, like those discussed in this paper, will be essential to the development of such procedures.

The paper is divided into four sections. In Sec. II we display the scattering anisotropy for dense random packing (DRP) models. We show projected atomic positions, density oscillations, and correlation functions associated with strong-scattering directions. In Sec. III we consider the scattering anisotropy for both the first and second diffraction rings for tetrahedrally bonded continuous-random-network (CRN) models. In Sec. IV we present results for scattering anisotropy from random points and show how these can be related

to results for the structural models.

II. DENSE RANDOM-PACKING MODELS

The scattering intensity per atom, in electron units, for a model structure with just one type of scatterer is given by

$$I(\vec{k}) = \frac{1}{N} \sum_{i,j} |f(k)|^2 e^{i \vec{k} \cdot (\vec{R}_i - \vec{R}_j)}$$

$$= \frac{|f|^2}{N} \left| \sum_i e^{i \vec{k} \cdot \vec{R}_i} \right|^2, \tag{1}$$

where $\vec{k}$ is the scattering vector, f is the atomic form factor, $\vec{R}_i$ and $\vec{R}_j$ are the positions of atoms i and j, and N is the number of atoms in the model. The form factor f is set equal to unity in all subsequent calculations. Another function of interest is the average of $I(\vec{k})$ over all directions of the scattering vector. This isotropic average scattering $\bar{I}$ thus depends only on $|k|$:

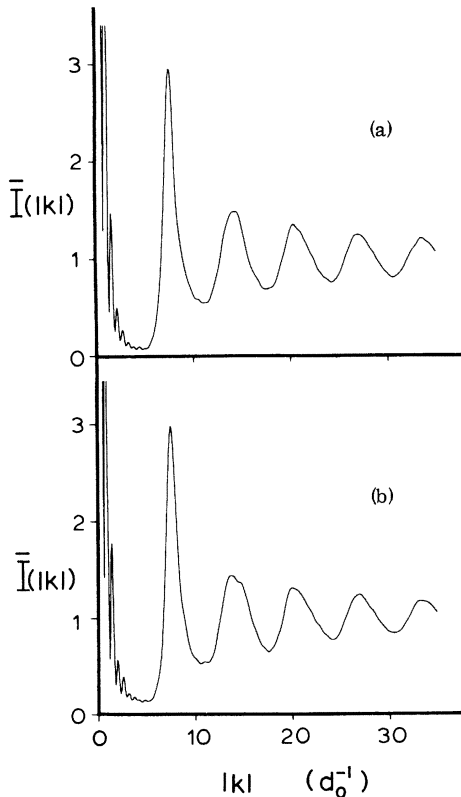$$\bar{I}(|k|) = \frac{1}{N} \sum_{ij} \frac{\sin |k| |R_i - R_j|}{|k| |R_i - R_j|} . \tag{2}$$

FIG. 1. Directionally averaged interference function $\bar{I}(|k|)$ for two DRP models. The scattering vector k is given in units of one divided by the hard-sphere diameter d_0. (a) 890 central units from a 3999-unit computer generated by Bennett. (b) 996 central units from a 7934-unit model hand built by Finney.
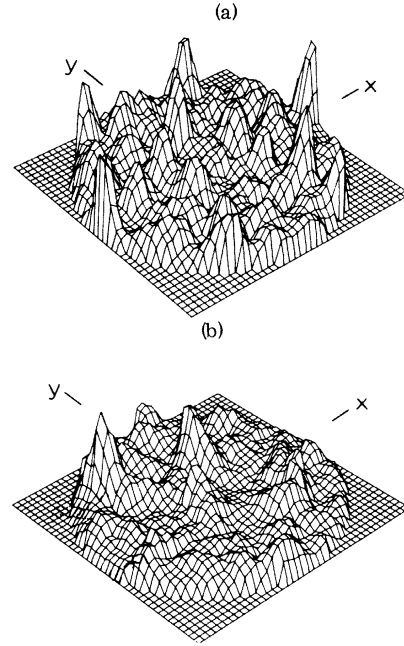

FIG. 2. Dependence of the interference function $I(\vec{k})$ on the direction of $\vec{k}$ for $|k| = 7.7\, d_0^{-1}$ for (a) the 890 central units of the DRP model of Bennett, and (b) the 996 central units of the DRP model of Finney. The spherical angles θ and φ giving the direction of $\vec{k}$ are obtained from x and y as follows: $\theta = \frac{1}{2}\pi(x^2 + y^2)^{1/2}$, $\phi = \tan^{-1}(y/x)$, where the region of nonzero $I(\vec{k})$ is corresponds to $x^2 + y^2 \leq 1$. The interference function has been averaged over directions within 5° of the indicated directions for purposes of illustration.

In Fig. 1 we show $\bar{I}(|k|)$ for spherical regions from two DRP models: (a) the 890 central units of the 3999-unit model of Bennett,[11] and (b) the 996 central units of the 7934-unit model of Finney.[10] The oscillations in $\bar{I}(|k|)$ at very small $|k|$ are related to the total model size. The first peak associated with correlations within the models occurs at $7.7\, d_0^{-1}$, where the distance unit d_0 is the hard-sphere diameter. The peak indicates the presence of structural periodicities with a spacing of $2\pi/7.7\, d_0^{-1} = 0.82\, d_0$, and the sharpness of the peak indicates that these periodicities persist over a considerable range [see Eq. (9)].

In Fig. 2 we display the behavior of the direction-dependent intensity function $I(\vec{k})$ with the direction of $\vec{k}$ for $|k| = 7.7\, d_0^{-1}$ for the two models. Points in the x, y plane correspond to the spherical angles θ and ϕ and the intensity is given by the height z of the "scattering net." To aid visualization of the results, we have averaged the scattering over an area of radius ~5° centered on the given directions. For each model there are several directions for which the scattering tends to be quite large.

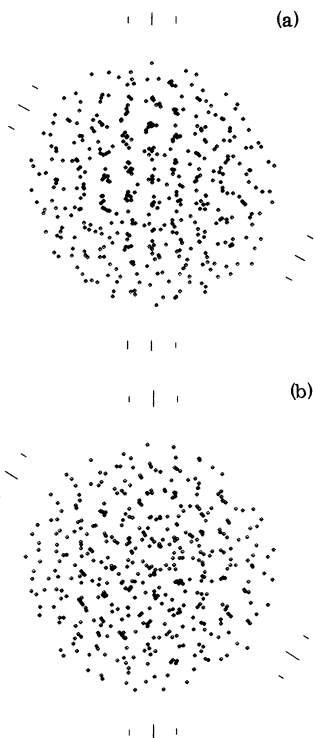In Fig. 3 we show the projection, for each mod-

These projected densities may be expressed in terms of the actual atomic density functions:

$$\rho(x, y, z) = \sum_{i=1}^{N} \delta(x - x_i)\delta(y - y_i)\delta(z - z_i),$$ (3)

where x_i, y_i, z_i are the coordinates of the ith atomic unit, and the z axis is chosen to be parallel to the scattering direction of interest. The projected density is then given by

$$P(z) = \int dx \int dy \, \rho(x, y, z).$$ (4)

Averaging $P(z)$ over successive intervals along z leads to the histogram form in Fig. 4. The oscillations in density are seen to be a large fraction of the average density and in some cases extend

FIG. 3. Projection of 440 central units of DRP models on the planes containing the two strongest scattering directions for $|k| = 7.7 \, d_0^{-1}$. The first few plane of high density and their spacing are indicated by the tick marks: (a) Bennett model, (b) Finney model. For case (a) there is a third set of planes perpendicular to a direction about midway between the directions perpendicular to the indicated sets of planes. The planes are most easily seen by tipping the page.

el, of the 440 atomic units closest to the center of gravity on the plane containing the *two* strongest scattering directions. As expected, we can observe (by tipping the page) that in each case there are planes of high density running perpendicular to both strong scattering directions. Note in particular that a large fraction of the units participate at once in more than one set of planes. For the model of Fig. 3(a) there are three strong scattering directions which are almost in the plane of the figure, the third direction being separated about 60° from each of the two directions indicated. In Fig. 2(a) these coplanar strong scattering directions correspond to the peaks near the periphery of the scattering net and are correlated to symmetry axes of a triangular 3 unit seed[11] which was used in generating the model.

The planes of high density apparent in Fig. 3 are shown quantitatively in Fig. 4. Here we give, in histogram form, the projected densities for the two strongest scattering directions for each of the two models.
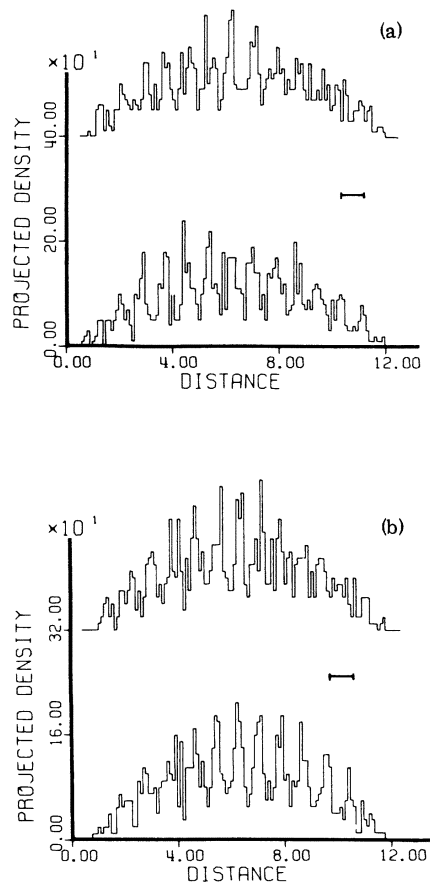

FIG. 4. Projected density, in units of atoms per sphere diameter, as a function of distance, measured in sphere diameters, along two strong-scattering directions for $|k| = 7.7 \, d_0^{-1}$ for DRP models. (a) 890 central units of Bennett model, (b) 996 central units of Finney model.] The plane spacing corresponding to this $|k|$ is $0.82 \, d_0$ and is indicated by the bars. The peak in the projected density correspond to planes of high density in the models. The upper curve of each pair has been displaced up by 320 units for clarity of presentation.
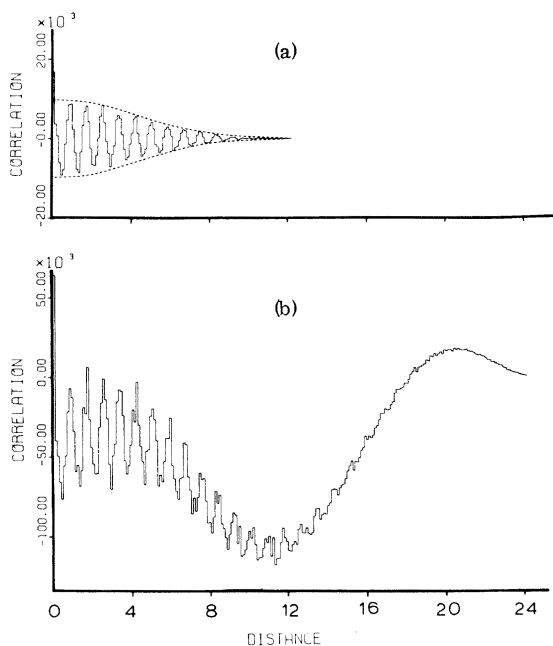
FIG. 5. Autocorrelation of the projected density for the strongest-scattering direction of the 996 central units of the Finney DRP model for $|k| = 7.7 \, d_0^{-1}$. The correlation is measured in units of atoms per hard-sphere diameter d_0, and distance is measured in units of d_0. A smooth background corresponding to a uniform finite sphere has been removed. (a) 996 central units of Finney model. The broken-line envelope shows the decrease in the autocorrelation due solely to the finite size of the model. (b) Full 7934 units of the Finney model. The broad oscillation is due to asphericity of the model. It is possible to discern 20 oscillations corresponding to a plane spacing of slightly more than $0.82d_0$.
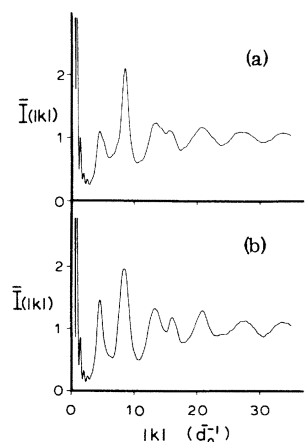

FIG. 6. Directionally averaged interference function $\bar{I}(|k|)$ for two CRN models. The wave vector k is given in units of one divided by the mean nearest-neighbor distance $\bar{d}_0$. (a) 563-unit model of Evans and Teter, modified from a band built model for SiO_2. (b) 519-unit of Polk, hand built, and then relaxed with the aid of a computer.
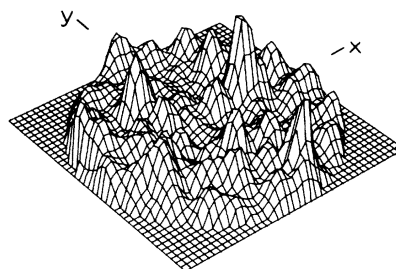

FIG. 7. Dependence of the interference function $I(\vec{k})$ on the direction of $\vec{k}$ for $|k| = 4.7 \, \bar{d}_0^{-1}$ for the 519-unit Polk model. The spherical angles θ and ϕ giving the direction of $\vec{k}$ are obtained for x and y as follows: $\theta = \frac{1}{2}\pi(x^2 + y^2)^{1/2}$, $\phi = \tan^{-1} y/x$, where the region of nonzero $I(\vec{k})$ corresponds to $x^2 + y^2 \le 1$. The interference function has been averaged over directions within 5° of the indicated directions for purposes of illustration. (Similar results have previously been presented in Ref. 18.)

across the entire model.

In Fig. 5(a) we show the autocorrelation function for the density oscillations for the strongest scattering direction discussed above for 996 central units of the Finney[10] model. This function is essentially a Patterson function projected on a line and may be expressed as follows:

$$G(z) = \int dz' \, P(z') P(z' + z) - \tfrac{3}{5}(N^2/a)$$

$$\times (1 - z/2a)^3 [1 + \tfrac{3}{2}z/a + \tfrac{1}{4}(z/a)^2], \qquad (5)$$

where the second term represents the Patterson function projected on a line for a uniform sphere of radius a, with the same volume and average density as the actual N unit cluster. This autocorrelation function is compared with the uniform sphere autocorrelation which dies off simply because fewer pairs of units can be found at larger separations in a finite cluster. Remarkably, the oscillatory correlation for this case falls off no faster than expected from finite size effects alone. In Fig. 5(b) we show a similar result for the full 7934-unit model, from which the 996-unit spherical cluster was taken. The autocorrelation function for this larger cluster does not oscillate about zero because the cluster does not have a spherical shape. We may note about 20 correlation peaks. Even for this large model the overall decrease in the correlation is not significantly more rapid than that due strictly to finite size.

III. TETRAHEDRALLY COORDINATED CONTINUOUS RANDOM NETWORK MODELS

In Fig. 6 we show $\bar{I}(|k|)$ for (a) the 563-atomic-unit CRN model built by Evans et al,[13] and (b) the 519-atomic-unit model of Polk.[12] The first peak in the isotropic intensity function is at $|k| = 4.7 \, d_0^{-1}$ where hence d_0 is the mean nearest-neighbor
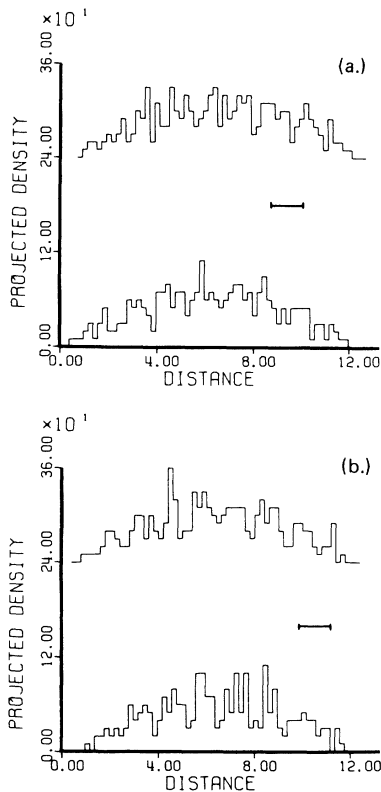
FIG. 8. Projected density, in units of atoms per bond length, as a function of distance, measured in bond length, along two strong scattering directions for $|k| = 4.7\, \bar{d}_0^{-1}$ for CRN models. The plane spacing corresponding to this $|k|$ is $2\pi/4.7\, \bar{d}_0^{-1} = 1.33\, \bar{d}_0$ and is indicated by the bars. The peaks in the projected density corresponds to planes of high density in the models. (a) 563-unit model of Evans and Teter, (b) 519-unit model of Polk. The upper curve of each pair has been displaced up by 240 units for clarity of presentation.

distance. The second and strongest peak is at $k = 8.7\, d_0^{-1}$. In Fig. 7 we show the anisotropy of the scattering for $|k| = 4.7\, d_0^{-1}$ for the Polk[12] model. We see here that there are many, almost equally strong peaks and also some considerable plateaulike regions. As first pointed out by Graczyk and Chaudhari,[3] these strong peaks are associated with density oscillations. These are shown quantitatively in Fig. 8 for two directions each in the two CRN models.

It might be asked if there is something special about the anisotropy in the scattering corresponding to the *first* peak in $\bar{T}|k|$. In fact this does not seem to be the case. In Fig. 9 we show the density oscillation corresponding to the strongest scattering direction for the second peak in $\bar{T}|k|$ for the 519-unit CRN model. Since the second peak is stronger than the first peak for this type of model, it is not surprising that the oscillations in projected density are in fact larger than any for the

first peak. They also persist across the entire model. Also, the strongest scattering direction for the second peak does not coincide with any of the strongest directions for the first peak.

IV. THEORY

In this section we outline a theory of *randomly occurring reinforcement and interference* which gives quantitatively accurate predictions for the magnitude of the scattering anisotropy of the model amorphous structures which have been studied. The key result is that even in a model where the intrinsic correlations are relatively short ranged and, on average, isotropic in character, it must be expected that by chance the correlations will persist over a much longer range for some directions. To demonstrate this we consider three cases: (i) a cluster of random scatterers, (ii) a single crystal, and (iii) superposed scattering from regions with short-range order. We then summarize the scattering anisotropy of various models in the light of the theory.

A. Random Scatterers

For the case of random scatterers (1) may be rewritten

$$I(\vec{k}) = \frac{1}{N}\left| \sum_{i=1}^{N} e^{i\gamma_i(\vec{k})} \right|^2 , \tag{6}$$

where the γ's are $\vec{k}$-dependent random phases for each scatterer. With $e^{i\gamma}$ represented by a unit vector in the complex plane, the sum in (6) may be treated as a random walk in two dimensions. $I(\vec{k})$ is then simply the square of the distance from the origin, divided by the number of steps. The distribution of values of I, for $N \gtrsim 10$ is a simple exponential,

$$P(I)\,dI = e^{-I}\,dI, \tag{7}$$

where $P(I)\,dI$ is the probability that I will fall in a range dI about a particular value I. The average of I is unity, $\int_0^\infty I P(I)\,dI = 1$, for all values of $\vec{k}$, a well-known result for random scatterers. However, the distribution (7) is not sharply peaked,
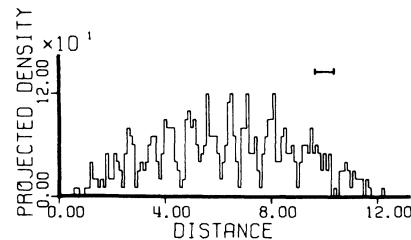

FIG. 9. Projected density for the strongest scattering direction for $|k| = 8.7\, \bar{d}_0^{-1}$ for the 519-unit Polk model The plane spacing corresponding to this $|k|$ is $0.72\, \bar{d}_0$ and is indicated by the bar.

even for large numbers of scatterers, because of chance constructive or destructive interference between even distantly separated scatterers. This somewhat surprising result does not conflict with experiments, which tend to yield reasonably consistent results for $I(\vec{k})$ for macroscopic disordered samples, because real experiments always involve a spread of scattering angles, and hence give averages over many different $I(\vec{k})$ measurements.

A related result obtained from (7) is that the variance of $I(\vec{k})$ does not decrease as the number of atoms in a random cluster is increased,

$$\langle I^2 \rangle - (\bar{I})^2 = 1. \tag{8}$$

However, this result must be interpreted with some care, for although the scattering does not become more isotropic as the cluster size grows, we expect that the angular width of maxima in $I(\vec{k})$, for fixed $|k|$, will decrease with increasing cluster size, i.e., the anisotropy will occur on a scale of increasing fineness. The full width at half-maximum Δk of a Bragg spot produced by a cube shaped crystal of edge length $\bar{R}$ is given by the Scherrer formula[2]

$$\Delta k = 5.6/\bar{R}, \tag{9}$$

and we employ this equation to estimate the number of *essentially independent* $I(\vec{k})$ values which occur for a random cluster as $\vec{k}$ varies in direction. For this purpose, $\bar{R}$ is taken to be the cube root of the volume which is occupied by the random cluster. We associate independent values of $I(\vec{k})$ only with values of $\vec{k}$ differing by at least the Δk given by (9). The number n of such independent values of $I(\vec{k})$ for all directions of $\vec{k}$ can be approximated by

$$n \sim 2\pi k^2/(5.6/\bar{R})^2 \sim 0.2 \ k^2\bar{R}^2, \tag{10}$$

where the numerator accounts for the degeneracy of $\vec{k}$ and $-\vec{k}$.

Sampling $I(\vec{k})$ on a grid of $\vec{k}$ values much coarser than Δk may miss significant maxima. Using a grid much finer than Δk should reveal no additional detail. For the calculations reported here we have taken a grid size such that the spacing between successive points is always less than $\frac{1}{2}\Delta k$. Note that the required number of sampling points increases both with the size of the model and with the magnitude of k.

For random clusters the distribution function (7) can be used to obtain an expression for the probability p' that the maximum of n independent values of $I(\vec{k})$ will be less than a certain value I',

$$p'(I') = (1 - e^{-I'})^n. \tag{11}$$

With (10) and (11), the expected range for the maximum value I_{max} of $I(\vec{k})$ for the fixed $|k|$ for a random cluster of characteristic dimension $\bar{R}$ can be obtained,

$$2 \ln |k|\bar{R} - 2.5 < I_{max}(|k|) < 2 \ln|k|\bar{R} + 0.5, \tag{12}$$

where the probabilities that I_{max} will be above or below this range are each about 0.1. The reason why I_{max} increases with $|k|\bar{R}$ is simply that the probability of finding a large intensity increases with the number of independent measurements. The directional average of $I(\vec{k})$, denoted $\bar{I}$ ($|k|$) is unity. Thus (12) may also be regarded as the expected range for the ratio $I_{max}/\bar{I}$. The above results for a finite cluster of random scatterers closely parallel the well studied case of a crystal with a large unit cell containing atoms positioned at random.[23,24]

B. Single Crystal

The scattering from a single crystal of finite size is a series of Bragg spots whose widths are given by (9). For a cube shaped crystal of N atoms and N unit cells, the maximum intensity for $|k|$ corresponding to a given spot is

$$I_{max}(|k|) = N. \tag{13}$$

The directionally averaged intensity may be shown to be

$$\bar{I}(|k|) = [\pi N/(|k|\bar{R})^2]m, \tag{14}$$

where m is the number of spots which occur for different directions of $\vec{k}$. It is of interest to note that the ration $I_{max}/\bar{I}$ increases as the $\frac{2}{3}$ power of the number of atoms in the structure. By contrast, for random scattering this ratio only increases as the logarithm of the number of atoms.

C. Short-range order

The scattering from the DRP and CRN models which we have studied does not correspond to that from well ordered crystals. Since $\bar{I}(|k|)$ has definite structure, the models are not completely random either. For these model structures, the question of greatest interest concerns scattering anisotropy where there is order, and where the intrinsic range of the order is comparable to or smaller than the size of the model.

We can address this question only in the following two simple cases. First, if the order corresponds to strict periodic correlations with a range much larger than the size of the model, then we recover the case of the single crystal. The second case occurs when the range of the order is short compared to the model size so that in any direction superimposed scattered waves are expected from several scattering regions. It can be shown that the intensity distribution in this case is describable by a two-dimensional random walk as in the case of random scatterers; the ratio $I_{max}(|k|)/$ $\bar{I}(|k|)$ derived for random scatterers should apply here also. It might be noted that this second case would apply to a sufficiently large polycrystalline

aggregate as well as to an amorphous sample which was much larger than the range of local correlations.

D. Results for model structures

In Table I are collected results for several structures; for each the directionally averaged scattering, the maximum scattering, the ratio of maximum to average scattering, and the expected ratio for random scattering are tabulated.

The first result is for a particular 519-atom cluster of scatterers randomly distributed within a sphere. The average density is the same as for the CRN model and $|k|$ corresponds to the first peak in $\bar{I}(|k|)$ for those models. Since the scatterers are all within a sphere, the scattering is not strictly described by the random scattering calculations. Still the ratio $I_{max}/\bar{I}$ is within the expected range. The over-all behavior of the anisotropy in $I(\vec{k})$ is shown in Fig. 10. Since the scatterers are randomly positioned in this model, we may say that there are no *intrinsic* correlations; there are no correlations associated with interactions among the atoms. Nonetheless, for directions corresponding to the maxima seen in Fig. 10, there must be periodic correlations in the projected atomic density, as anticipated by the analysis of Sec. IV A.

The second result in Table I is for the 519-atom CRN model with $|k|$ corresponding to the first peak in $\bar{I}(|k|)$. Somewhat surprisingly, the maximum anisotropy for the scattering is almost within the range expected for random reinforcement from intrinsic correlations whose range is much less than the size of the model. Also the over-all character of the anisotropy in the scattering appears to us to be not very different from that for
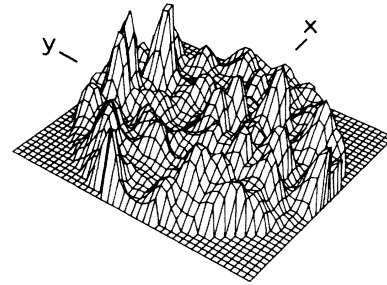

FIG. 10. Dependence of the interference function $I(\vec{k})$ on the direction of $\vec{k}$ for $|k| = 4.7\, \bar{d}_0^{-1}$ for a spherical cluster of 519 randomly placed scatterers. (Here, $\bar{d}_0$ is interpreted as the bond length in a diamond cubic structure crystal with the same density as this random model.) The spherical angles θ and ϕ giving the direction of $\vec{k}$ are obtained for x and y as follows: $\theta = \frac{1}{2}\pi(x^2 + y^2)^{1/2}$, $\phi = \tan^{-1}y/x$, where the region of nonzero $I(\vec{k})$ corresponds to $x^2 + y^2 \leq 1$. The interference function has been averaged over directions within 5° of the indicated directions for purposes of illustration.

random scattering, as may be seen by comparing Figs. 7 and 10. Lines 3, 4, and 5 of Table I give similar results for other CRN models, with this same value of $|k|$. The next result is for the 519-atom CRN model with $|k|$ corresponding to the second peak in $\bar{I}(|k|)$. The anisotropy here is somewhat higher than would be expected for random scattering. [An examination of the angular dependence of the scattering (not shown) reveals only one particularly large peak.]

Results for the two DRP models for $|k|$ corresponding to the first peak in $\bar{I}(|k|)$, lines 7 and 8 of Table I, are again indicative of the presence of intrinsic order comparable to the model size, since the maximum scattering is somewhat outside the range for purely random scattering. At the other extreme, results for these models may be compared with those for a perfect face-centered cubic crystal of comparable size—the last entry in Table I. The average scattering $\bar{I}$ for such a crystal is not dramatically greater than for the models; however, the anisotropy for the single crystal is truly enormous, despite there being eight equivalent (111) Bragg spots for this $|k|$. For the DRP models as well as for the CRN models, the quantitative magnitude of scattering anisotropy can be largely accounted for by chance reinforcement and interference, as exist in random clusters, and is quite different from the anisotropy expected for a well-defined periodic structure.

ACKNOWLEDGMENTS

TABLE I. Characteristics of the scattering anisotropy for various model structures. Except as otherwise indicated, the magnitude of the scattering vector corresponds to the first diffraction ring.

		$\bar{I}$	I_{max}	$\dfrac{I_{max}}{\bar{I}}$	$\left(\dfrac{I_{max}}{\bar{I}}\right)_{Random}$
1	519-Random[a]	0.92	7.3	7.9	6.6 ± 1.5
2	519-CRN	1.47	12.3	8.3	6.6 ± 1.5
3	201-CRN	1.21	9.8	8.1	5.9 ± 1.5
4	500-CRN	1.61	12.4	7.7	6.5 ± 1.5
5	563-CRN	1.09	8.8	8.1	6.6 ± 1.5
6	519-CRN[b]	1.95	19.7	10.1	7.8 ± 1.5
7	996-DRP	2.93	38.9	13.3	7.6 ± 1.5
8	890-DRP	2.93	33.5	11.4	7.5 ± 1.5
9	864-fcc	5.09	864.0	169.8	7.4 ± 1.5

[a]The scattering vector corresponds to the first diffraction ring of CRN models.

[b]The scattering vector corresponds to the second diffraction ring.

zyk, and P. Chaudhari for helpful discussions. We are particularly grateful to W. Cochran for

helpful comments on the theory of intensity statistics.

[1]F. Zernike and J. A. Prins, Z. Phys. 41, 184 (1972).

[2]B. E. Warren, X-ray Diffraction (Addison-Wesley, Reading, 1969).

[3]J. F. Graczyk and P. Chaudhari, Phys. Status Solidi B 58, 163 (1973).

[4]M. L. Rudee and A. Howie, Philos. Mag. 25, 1001 (1972).

[5]P. Chaudhari, J. F. Graczyk, and S. R. Herd, Phys. Status Solidi B 51, 801 (1972).

[6]S. R. Herd and P. Chaudhari, Phys. Status Solidi A 26, 627 (1974).

[7]W. Cochran, in Tetrahedrally Bonded Amorphous Semiconductors, edited by M. H. Brodsky, S. Kirkpatrick, and D. Weaire (AIP, New York, 1974), p. 177.

[8]M. V. Berry and P. A. Doyle, J. Phys. C 6, L6 (1973).

[9]O. L. Krivanek and A. Howie, J. Appl. Crystallogr. 8, 213 (1975).

[10]J. L. Finney, Proc. R. Soc. Lond. A 319, 479 (1970).

[11]C. H. Bennett, J. Appl. Phys. 43, 2727 (1972).

[12]D. E. Polk, J. Non-Cryst. Solids 5, 365 (1971).

[13]D. L. Evans, M. P. Teter, and N. F. Borelli, in Tetrahedrally Bonded Amorphous Semiconductors, edited by M. H. Brodsky, S. Kirkpatrick, and D. W Weaire (AIP, New York, 1974), p. 218.

[14]D. S. Boudreaux, D. E. Polk, and M. G. Duffy, in Tetrahedrally Bonded Semiconductors, edited by M. H. Brodsky, S. Kirkpatrick, and D. Weaire (AIP, New York, 1974), p. 206.

[15]P. Steinhardt, R. Alben, and D. Weaire, J. Non-Cryst. Solids 15, 199 (1974).

[16]N. J. Shevchik, Phys. Status Solidi 52, K121 (1972).

[17]P. Chaudhari, J. F. Graczyk, and H. P. Charbnau, Phys. Rev. Lett. 29, 452 (1972).

[18]P. Chaudhari and J. F. Graczyk, in Amorphous and Liquid Semiconductors, edited by J. Stuke and W. Brenig (Taylor and Frances, London, 1974), p. 59.

[19]P. Chaudhari, J. F. Graczyk, and S. R. Herd, NATO Conference, University of Rhode Island, 1974 (unpublished); and IBM Research Report No. 5246, 1975 (unpublished).

[20]J. F. Graczyk and P. Chaudhari, Phys. Status Solidi B 58, 501 (1973).

[21]J. F. Graczyk and P. Chaudhari, IBM Research Report No. 4491, 1973 (unpublished).

[22]J. F. Graczyk and P. Chaudhari, J. Non-Cryst. Solids 17, 299 (1975).

[23]A. J. C. Wilson, Acta Crystallogr. 2, 318 (1949).

[24]See also H. Lipson and W. Cochran, The Determination of Crystal Structures (Bell, London, 1966), Chap. 3.